Comparison of multifragmentation dynamical models

J. Rizzo,[1,2] M. Colonna,[1,2] and A. Ono[3]
[1]*LNS-INFN, I-95123 Catania, Italy*
[2]*Physics and Astronomy Department, University of Catania, Italy*
[3]*Department of Physics, Tohoku University, Sendai 980-8578, Japan*
(Received 18 September 2006; published 27 August 2007)

Multifragmentation scenarios, as predicted by antisymmetrized molecular dynamics (AMD) or momentum-dependent stochastic mean-field (BGBD) calculations are compared. Whereas in the BGBD case fragment emission is clearly linked to the spinodal decomposition mechanism (i.e., to mean-field instabilities), in AMD many-body correlations have a stronger impact on the fragmentation dynamics. In fact, the density and momentum fluctuations develop earlier in AMD, suggesting that fragments are formed on shorter time scales in AMD, on about equal footing as light-particle pre-equilibrium emission.

DOI: 10.1103/PhysRevC.76.024611 PACS number(s): 25.70.Pq, 24.10.Lx, 24.10.Pa

I. INTRODUCTION

During the past decade, multifragmentation (i.e., the breakup of excited nuclear systems into many pieces) has been extensively investigated in heavy-ion collisions (HIC) around Fermi energies, both from the experimental and theoretical points of view [1–9]. In particular, the study of the mechanism responsible for fragment production has received much attention, especially in relation to the possibility of observing a liquid-gas phase transition in nuclei [1–5]. Many efforts have been devoted to the characterization of the properties of the fragmenting source, such as temperature and density, to determine its location inside the nuclear matter phase diagram.

Because of compression and/or thermal effects, the composite systems formed in HIC may reach low density values, attaining the coexistence zone of the nuclear matter phase diagram. For instance, an excited system that expands under the conditions of thermal equilibrium could perform a phase transition, staying close to the liquid branch of the coexistence line [2,10]. However, owing to Coulomb instabilities, the limiting temperature that a nucleus can sustain as a compact configuration may be lower than the critical temperature [11]. In this situation, the system is brought inside the coexistence zone of the nuclear matter phase diagram and undergoes a spontaneous phase separation, breaking up into several fragments [4,7].

It is generally believed that in central HIC at Fermi energies, the composite matter can be compressed up to twice the normal density value (as revealed for instance by the emission of energetic particles through hard two-body scattering [12]), and then the system expands and breaks up into many pieces [5–7]. One of the most challenging and still open questions is the understanding of the fragmentation mechanism along this path. The decompression following the initial collisional shock should be strong enough to push the system inside the unstable region of the phase diagram and fragments could be formed as mean-field spinodal instabilities develop [5,7]. However, nucleon correlations are expected to be rather large in the high-density phase, owing to the huge number of two-body nucleon-nucleon collisions. Hence some memory of these high-density correlations could be kept along the fragment formation process.

According to classical molecular dynamics [13,14] or lattice-gas calculations [15], self-bound clusters are observed, even at equilibrium, in high-density systems. This has recently suggested an interpretation of the multifragmentation phenomenon in terms of a sudden explosion of the system, where pre-fragments start to appear already in the high-density phase and subsequently fly apart from each other owing to the strong Coulomb repulsion [16]. However, one should keep in mind that this clustering effect revealed in the high-density phase could be much stronger in classical systems than in nuclear matter, which is a Fermi liquid. For instance, mean-field calculations of the response of nuclear matter to the presence of density fluctuations show that correlations constructed in the high-density phase are damped. Indeed, according to a mean-field description, it is not energetically convenient for a Fermi system at density larger than the normal value to develop these high-density bumps [7].

However, if many fluctuations are present in the high-density stage of the reaction, and the system expands rather quickly, these correlations could survive and play an important role in determining the properties of the formed fragments. In contrast, if the size of fluctuations is not so large, these structures could be reorganized again by the low-density unstable mean field.

Hence it is clear that the fragmentation mechanism is very sensitive to the delicate balance among many-body correlations, mean-field effects, and the time scale imposed by the reaction dynamics, especially in the Fermi energy domain, where one- and two-body effects are equally important. Therefore, depending on the way one treats the different effects, one could expect a different outcome from the available theoretical models describing multifragmentation. In this paper we undertake this kind of investigation, by comparing the results given by two fragmentation models: the stochastic mean-field model, including momentum dependence (BGBD) [17], and the antisymmetrized molecular dynamics (AMD) model [6]. Both have proved to give a good reproduction of some aspects of multifragmentation data [18,19]. We analyze central reactions, where we expect to see larger dynamical

(compression-expansion) effects on fragment formation. The present study will allow us to get a deeper insight into the reaction mechanism, in connection with the ingredients of the two models. This should be reflected in the properties of the obtained primary fragments and eventually on measured observables. In this way one can also try to identify the experimental quantities that are more sensitive to the fragmentation scenario. The paper is organized as it follows: In Sec. II we will give an outlook of the main ingredients of both models. In Sec. III we study the fragmentation path, as given by the two models, in the case of a central reaction, ^{112}Sn + ^{112}Sn at 50 MeV/nucleon [8]. Conclusions are drawn in Sec. IV.

II. INGREDIENTS OF THE MODELS

Two different kinds of microscopic approaches have been proposed and applied to study heavy-ion reaction mechanisms (i.e., to describe the dynamics of nuclear many-body systems). One is the class of molecular dynamics models [20–24]; the other is represented by stochastic mean-field approaches [7,25,26].

In the mean-field class of descriptions, the dynamical state of the nuclear system is characterized by the reduced one-body density in phase space, $f(\mathbf{r}, \mathbf{p}, t)$, the classical analog of the Wigner transform of the one-particle density matrix. At low energies, the time evolution of the one-body density is governed by the Vlasov equation, which can be regarded as the semiclassical approximation to the time-dependent Hartree-Fock theory. The residual direct collisions between the constituent nucleons are incorporated by means of a Pauli-blocked collision integral, leading to the so-called Boltzmann-Uehling-Uhlenbeck (BUU) or Boltzmann-Nordheim-Vlasov (BNV) approaches [27,28]. The stochastic extension of the transport treatment for the one-particle density is obtained by introducing a stochastic term representing the fluctuating part of the collision integral [25], in close analogy with the Langevin equation for Brownian motion.

Molecular dynamics models usually assume a fixed Gaussian shape for the single-particle wave functions. The many-body state is represented by a simple product wave function, with or without antisymmetrization. In this way, though single-particle wave functions are supposed to be independent (mean-field approximation), the use of localized wave packets induces many-body correlations both in mean-field propagation and hard two-body scattering (collision integral), which is treated stochastically. From the point of view of stochastic mean-field models, the philosophy of molecular dynamics would be to introduce a special kind of fluctuation by stochastically localizing the single-particle wave functions.

In the following we will give the ingredients of the two models, which can be seen as representative of each class that we consider in the present work.

A. BGBD

The stochastic mean-field model considered here is a semiclassical nonrelativistic transport approach, of BNV type (see Refs. [29,30]), that uses an isospin- and momentum-dependent effective interaction. The latter is derived via an asymmetric extension of the Gale-Bertsch-Das Gupta (GBD) force [31,32].

The energy density can be parametrized as follows (see also Refs. [33,34]):

$$\varepsilon = \varepsilon_{\rm kin} + \varepsilon(A', A'') + \varepsilon(B', B'') + \varepsilon(C', C''), \qquad (1)$$

where $\varepsilon_{\rm kin}$ is the usual kinetic energy density and

$$\begin{aligned} \varepsilon(A', A'') &= (A' + A''\beta^2)\frac{\rho^2}{\rho_0}, \\ \varepsilon(B', B'') &= (B' + B''\beta^2)\left(\frac{\rho}{\rho_0}\right)^{\sigma}\rho, \\ \varepsilon(C', C'') &= C'(\mathcal{I}_{NN} + \mathcal{I}_{PP}) + C''\mathcal{I}_{NP}. \end{aligned} \qquad (2)$$

The variable $\beta = (N - Z)/A$ defines the isospin content of the system, given the number of neutrons (N), protons (Z), and the total mass $A = N + Z$; the quantity ρ_0 is the normal density of nuclear matter. The momentum dependence is contained in the $\mathcal{I}_{\tau\tau'}$ terms, which indicate integrals of the form

$$\mathcal{I}_{\tau\tau'} = \int d\vec{p}\, d\vec{p}\,' f_\tau(\vec{r}, \vec{p}) f_{\tau'}(\vec{r}, \vec{p}\,') g(\vec{p}, \vec{p}\,'),$$

where $g(\vec{p}, \vec{p}\,') = 1/[1 + (\vec{p} - \vec{p}\,')^2/\lambda]$ and f_τ represents the one-body distribution function of neutrons or protons. Here λ is a constant, which is taken equal to $(1.5\, k_F)^2$, with k_F the Fermi momentum at normal density. This choice of the function $g(\vec{p}, \vec{p}\,')$ gives a similar behavior with respect to the Gogny effective interaction used in the AMD simulations (see next section). We use a soft equation of state for symmetric nuclear matter [compressibility modulus $K_{\rm NM}(\rho_0) = 215$ MeV]. In this frame we can easily adjust the parameters to fix the density dependence of effective mass and symmetry energy.

We describe the time evolution of the system in terms of the one-body distribution function $f_\tau(\mathbf{r}, \mathbf{p}, t)$, as ruled by the nuclear mean-field (plus Coulomb interaction for protons) and hard two-body scattering, according to the so-called Boltzmann-Langevin equation [25,26],

$$\frac{df_\tau}{dt} = \frac{\partial f_\tau}{\partial t} + \{f_\tau, H\} = I_\tau[f] + \delta I_\tau[f], \qquad (3)$$

where $H(\mathbf{r}, \mathbf{p}, t)$ is the one-body Hamiltonian, $I_\tau[f]$ is the average two-body collision integral, and $\delta I_\tau[f]$ represents the stochastic source term [7,25,26]. The test-particle method is used to solve Eq. (3) numerically. Each test particle is associated with a wave packet (of triangular shape) with width equal to 0.85 fm. The free-energy- and angle-dependent nucleon-nucleon cross section is used in the collision integral. Fluctuations are introduced within this mean-field treatment, according to the approach presented in Refs. [29,35] (i.e., by agitating the spatial density profile). Once local thermal equilibrium is reached, the density fluctuation amplitude σ_ρ is evaluated by projecting on the coordinate space the kinetic equilibrium value of a Fermi gas. Then, in the cell of $\mathbf{r}$ space being considered, the density fluctuation $\delta\rho$ is selected randomly according to the Gaussian distribution $\exp(-\delta\rho^2/2\sigma_\rho^2)$. This determines the variation of the number of particles contained in the cell. A few leftover particles are randomly distributed again to ensure conservation of mass.

Momenta of all particles are finally slightly shifted to ensure momentum and energy conservation. Hence, although the dynamical evolution of the system is still described in terms of the one-body distribution function, this function experiences a stochastic evolution, in response to the action of a fluctuation term essentially determined by the degree of thermal agitation present in the system.

According to this stochastic mean-field theory, the fragmentation process is dominated by the growth of volume (spinodal) and surface instabilities encountered during the expansion phase of the considered excited systems [36]. Therefore density fluctuations provide the seeds of the formation of fragments, whose characteristics are related to the properties of the most unstable collective modes of the mean field. In finite nuclei, several multipoles are excited with close probabilities. Hence a large variety of fragment configurations may be obtained, owing to the beating of the several unstable modes [5,7,36]. This description of the fragmentation path can explain several features, concerning also rather exclusive observables [5], observed in experimental data at around 30 MeV/nucleon [19].

B. AMD

For the AMD [18,22,37] calculations presented here, we use the same framework as in Ref. [18], which can reproduce the fragment charge distribution of the central Xe + Sn collisions at 50 MeV/nucleon.

In AMD, we employ the Slater determinant of Gaussian wave packets,

$$\langle \mathbf{r}_1 \dots \mathbf{r}_A | \Phi(Z) \rangle \propto \det_{ij} [\exp\{-\nu(\mathbf{r}_i - \mathbf{Z}_j/\sqrt{\nu})^2\} \chi_{\alpha_j}(i)], \quad (4)$$

where χ_{α_i} are the spin-isospin states with $\alpha_i = p\uparrow, p\downarrow, n\uparrow,$ or $n\downarrow$. Thus the many-body state $|\Phi(Z)\rangle$ is parametrized by a set of complex variables $Z \equiv \{\mathbf{Z}_i\}_{i=1,\dots,A}$, where A is the number of nucleons in the system. The width parameter $\nu = (2.5\ \text{fm})^{-2}$ is treated as a constant parameter common to all the wave packets. If we ignore the antisymmetrization effect, the real part of $\mathbf{Z}_i$ corresponds to the position centroid and the imaginary part corresponds to the momentum centroid. This choice of wave functions is suitable to describe fragmentation channels where each single-particle wave function should be localized within a fragment.

The dynamics of fragmentation is a highly complicated quantum many-body problem in which a huge number of fragmentation channels will appear in the course of the evolution. An AMD wave function [Eq. (4)] is intended to describe one of the channels rather than the total many-body state, and the emergence of channels is represented approximately by some stochastic terms in the equation of motion.

The stochastic equation of motion for the wave packet centroids Z may be symbolically written as

$$\frac{d}{dt}\mathbf{Z}_i = \{\mathbf{Z}_i, \mathcal{H}\}_{\text{PB}} + (NN\ \text{coll}) + \Delta\mathbf{Z}_i(t) + \mu(\mathbf{Z}_i, \mathcal{H}'). \quad (5)$$

The first term, $\{\mathbf{Z}_i, \mathcal{H}\}_{\text{PB}}$, is the deterministic term derived from the time-dependent variational principle with an assumed effective interaction such as the Gogny interaction [38]. The second term represents the effect of the stochastic two-nucleon collision process. The collisions are performed with the "physical nucleon coordinates" that take account of the antisymmetrization effects, and then the Pauli blocking in the final state is automatically introduced [22]. The third term, $\Delta\mathbf{Z}_i(t)$, is a stochastic fluctuation term that has been introduced to respect the change of the width and shape of the single-particle distribution [6,18,39]. In other words, the combination $\{\mathbf{Z}_i, \mathcal{H}\}_{\text{PB}} + \Delta\mathbf{Z}_i(t)$ approximately reproduces the prediction by mean-field theories for the ensemble-averaged single-particle distribution, while each nucleon is localized in phase space for each channel. The term $\Delta\mathbf{Z}_i(t)$ is calculated practically by solving the Vlasov equation with the same effective interaction as for the term $\{\mathbf{Z}_i, \mathcal{H}\}_{\text{PB}}$. In the present version of AMD [18], the property of the fluctuation $\Delta\mathbf{Z}_i(t)$ is chosen in such a way that the coherent single-particle motion in the mean field is respected for some time interval until the nucleon collides with another nucleon. The last term, $\mu(\mathbf{Z}_i, \mathcal{H}')$, is a dissipation term related to the fluctuation term $\Delta\mathbf{Z}_i(t)$. The dissipation term is necessary to restore the conservation of energy that is violated by the fluctuation term. The coefficient μ is given by the condition of energy conservation. However, the form of this term is somewhat arbitrary. We shift the variables Z to the direction of the gradient of the energy expectation value $\mathcal{H}$ under the constraints of conserved quantities (the center-of-mass variables and the total angular momentum) and global one-body quantities (monopole and quadrupole moments in coordinate and momentum spaces). A complete formulation of AMD can be found in Refs. [18,37].

In the present work, we use the Gogny effective interaction [38] that corresponds to a soft equation of state of symmetric nuclear matter with incompressibility $K_{\text{NM}}(\rho_0) = 228$ MeV. The mean field for this force has a momentum dependence that is similar to that in the BGBD calculation. As the two-nucleon collision cross sections ($\sigma_{pp} = \sigma_{nn}$ and σ_{pn}), we use the energy- and angle-dependent values in free space with a maximum cutoff of 150 mb. To avoid low-energy spurious collisions, resulting from Pauli blocking violation (caused by the finite number of test particles), in the BGBD calculations a lower cutoff, 50 mb, has been considered. We have checked that this does not affect significantly the degree of stopping reached in the calculations.

C. Some remarks

We would like to stress here the main differences between the two models.

In the AMD version used here [18], a special procedure is adopted that ensures a coherent single-particle motion in the mean field (including diffusion and shrinking effects of the nucleon wave packet in phase space) until the considered nucleon collides another one. It can be demonstrated that this procedure reproduces exactly the coherent time evolution of the Wigner function f in the case of a harmonic oscillator potential (or for free nucleons), though this correspondence is not exact in the general case. Hence one-body effects should be similarly treated in the two models. From this point of

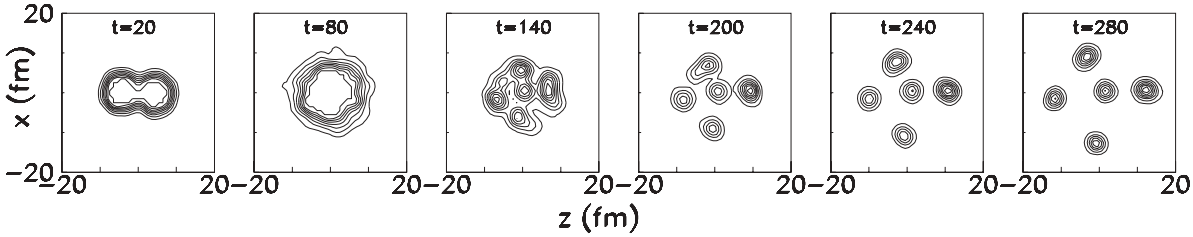

FIG. 1. Contour plots of the density projected on the reaction plane calculated with BGBD for the central reaction ^{112}Sn + ^{112}Sn at 50 MeV/nucleon, at several times (fm/c). The size of each box is 40 fm.

view, the present version of AMD is rather different from earlier molecular dynamics formulations [20,22], where the use of localized wave packets in the full dynamics implies that one-body effects are not as precisely described as in mean-field models.

The most relevant difference between AMD and BGBD is related to the method followed to implement stochastic two-body scattering. In fact, in BGBD, fluctuations are introduced by agitating the one-body density function, to account for the stochastic part of the collision integral, according to the Boltzmann-Langevin theory [7,25]. In some sense, this would correspond to a description of the system in terms of unrestricted fluctuating single-particle wave functions. On the other side, in AMD, fluctuations are introduced by stochastically localizing the single-particle wave functions in phase space when a two-nucleon collision takes place.

It is difficult to discuss the general validity of the various approximations adopted to solve the quantum many-body dynamics because it may depend on the particular reaction mechanism and energy range under study. Here we will focus on the description of the multifragmentation mechanism at 50 MeV/nucleon. Although it is well known that the results of early molecular dynamics models [20,22] and standard mean-field approaches [28] are rather different, the improved AMD and the stochastic BGBD can be considered as closer approaches and it is interesting to investigate how their respective predictions compare to each other in the case of fragmentation reactions.

III. ANALYSIS OF THE RESULTS

Our aim is to investigate the fragmentation path in violent collisions at intermediate energy, as predicted by the BGBD and the AMD models. As already discussed, in the BGBD model one essentially follows the evolution of the one-body density, and the fragmentation mechanism is mainly based on the amplification of its fluctuations. In AMD, nucleon wave packets are propagated, from which, however, it is possible to reconstruct the one-body density and related observables.

Hence our study of the reaction path will be performed by looking at quantities connected to the one-body density and to its fluctuations. We will investigate central collisions of the system ^{112}Sn + ^{112}Sn at 50 MeV/nucleon. An ensemble of 200 trajectories with $b = 0.5$ fm has been collected with BGBD, and in AMD 20 events with $0 < b < 1$ fm are considered.

A. One-body observables

To give a qualitative representation of the time evolution of the system, density contour plots in the reaction plane, as obtained in the two models, are shown in Figs. 1 and 2 at several time steps. As one can see from the figures, both models predict that the system is initially compressed. Then expansion follows and several intermediate mass fragments (IMF) appear.

The degree of stopping reached in the two calculations is rather similar, as shown in Fig. 3, where rapidity distributions are compared for the two models. A slightly larger transparency is observed in the BGBD case, probably due to small differences in the effective forces employed in the two codes, as previously explained, and/or a different impact of many-body correlations on the average evolution.

In BGBD, according to the value of the spatial density $\rho(\mathbf{r})$, one can identify a "gas" phase ($\rho < \rho_0/6$, where ρ_0 denotes the normal density value), associated with particles that rapidly leave the system (pre-equilibrium emission) and/or are evaporated, and a "liquid" phase, where fragments belong to the system. In fact, we observe that, after a clusterization

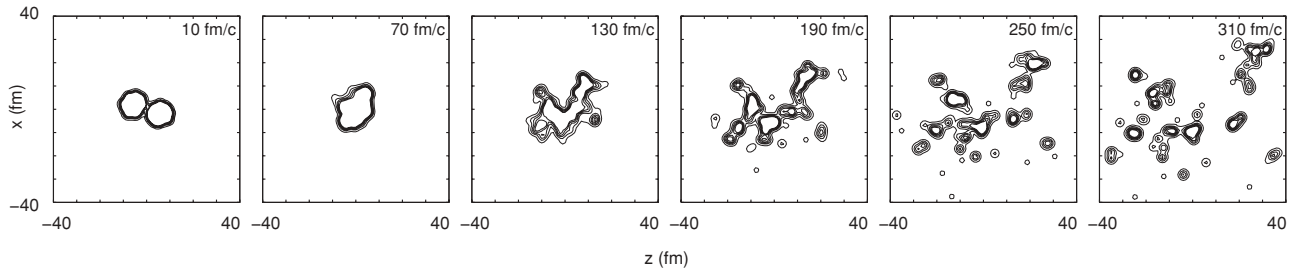

FIG. 2. The same as in Fig. 1 but calculated with AMD. The size of each box is 80 fm.

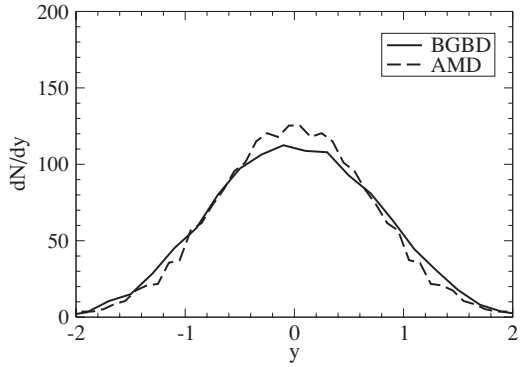

FIG. 3. Rapidity distribution as obtained in the central reaction ^{112}Sn + ^{112}Sn at 50 MeV/nucleon at the final time. The solid curve refers to BGBD calculations; the dashed curve represents AMD calculations.

procedure has been applied [29], the "liquid" essentially corresponds to particles with mass greater than 4, whereas these particles are absent in the "gas" phase. Hence, in AMD the fragments with $A \leqslant 4$ are regarded as in the gas part. The time evolution of the number of nucleons that are in the gas phase is represented in Fig. 4. It is possible to observe that the number of particles that escape at early times from the interacting nuclear matter, as a result of two-body scattering (pre-equilibrium effects), is different in the two models. In the BGBD case (solid curve) the emission rate is larger with respect to the AMD calculations. Moreover, there is a clear change of slope at around $t \approx 100$ fm/c, where, as we will see in the following (see also Fig. 1), the nuclear system reaches low density values, fragments start to be formed, and nucleons are emitted by essentially evaporative processes. This is not so evident in the AMD case. The total mass that goes into very light particles ($A \leqslant 4$) is smaller in the AMD case, pointing to more efficient clustering effects.

To closely follow the time evolution of the system and to better characterize its fragmentation path, we have studied the behavior of the following observables: the radial density

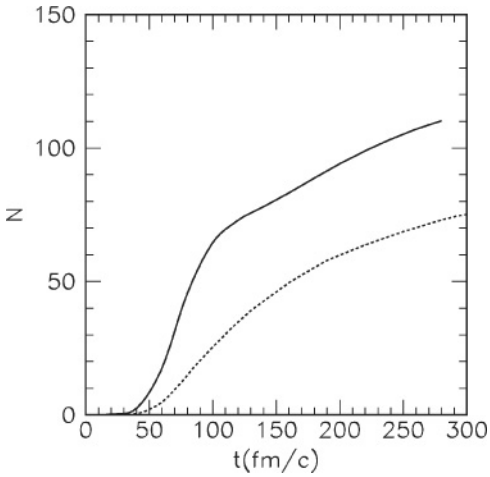

FIG. 4. Time evolution of the number of nucleons in the "gas" phase. The solid curve refers to BGBD calculations; the dashed curve represents AMD calculations.

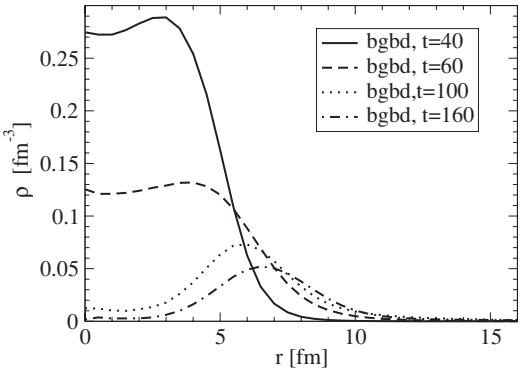

FIG. 5. Density profiles, at several times (in fm/c), as obtained in the BGBD case.

profile of the system and the radial collective momentum as functions of time. The radial density at a given distance r is obtained by averaging the local density $\rho(\mathbf{r})$ over the surface of a sphere of radius r. The radial collective momentum is the projection of the collective momentum at the position $\mathbf{r}$ along the radial direction, averaged over the surface of the sphere of radius r. These quantities are further averaged over the event ensemble.

In the BGBD case, the behavior of the radial density profile, presented in Fig. 5, indicates that, after an initial compression ($t = 40$ fm/c), the system expands and finally it gets rather dilute, owing to the occurrence of a monopole expansion, generated by the compression. As one can see from Fig. 1, while the system expands, it breaks up into many pieces. The matter appears mostly concentrated within a given window of the radial distance (see for instance the line at $t = 100$ fm/c), indicating the formation of a bubble-like configuration, where fragments are located. Indeed, the central region of the system is rapidly depleted. This behavior was already discussed in the context of BUU calculations [40], where it was found that, under suitable conditions, an initially compressed nuclear system expands into a hollow, quasi-stationary unstable configuration.

It is rather interesting to look at the profile of the collective momentum (divided by the nucleon mass), $v(r)$(see Fig. 6). The time evolution of this quantity is largely influenced by the occurrence of monopole compression and expansion. Indeed,

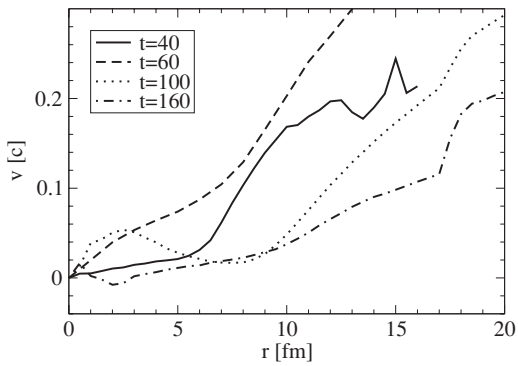

FIG. 6. Collective momentum profiles, in units of the nucleon free mass, at several times (in fm/c), as obtained in the BGBD case.

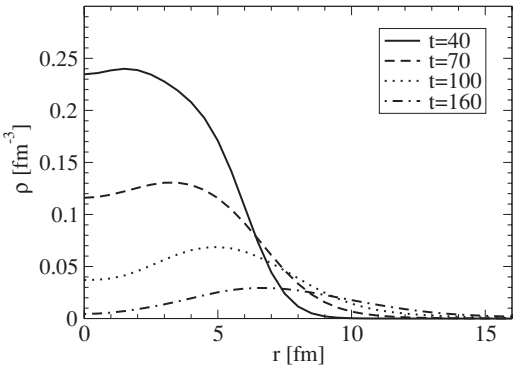

FIG. 7. Density profiles, at several times (in fm/c), as obtained in the AMD case.

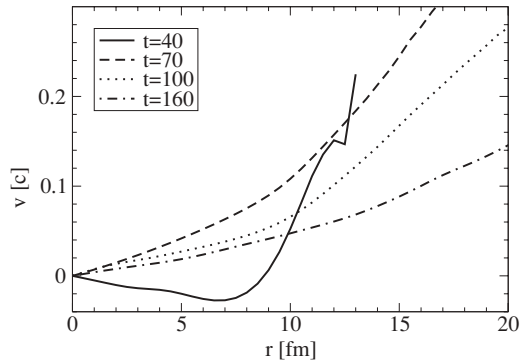

FIG. 8. Collective momentum profiles, in units of the nucleon free mass, at several times (in fm/c), as obtained in the AMD case.

after the initial compression, the restoring force generated by the mean field pushes the system back to the normal density value and the collective momentum increases (compare the evolution from $t = 40$ to 60 fm/c). It can be noticed that, at $t = 60$ fm/c, in the region where the "liquid" is located (i.e., for $r < 8$–9 fm; cf. Fig. 5), the collective momentum profile is almost self-similar; that is, the radial momentum is proportional to the radial distance. Then the system goes into the expansion phase and the collective momentum decreases again. This deceleration indicates that the system is still rather homogeneous while it expands, reaching the low-density (unstable) region. More specifically, the system slows down because of the presence of a counterstreaming flow that develops from the surface toward the interior, which tries to recompact the system. As seen before, as the system approaches the dilute turning point, the density profile becomes drastically distorted into a bubble-like configuration, as a result of the competition between the monopole radial expansion and the effects of the nuclear cohesion at dilute density [40]. Local density and temperature conditions correspond to a phase point well within the region of mechanical instabilities. Then fragmentation can be associated with the occurrence of spinodal decomposition [7]. At the same time, the collective momentum profile is modified and, in the region where the matter is located (cf. Fig. 5), the system is slowed down. So actually when fragments start to appear ($t \approx 100$ fm/c) their collective momentum is not so large. However, the momentum is rather large in the central part of the system ($r < 3$ fm at $t = 60$ and 100 fm/c), which is related to the rapid depletion of the density in this region.

One may also notice that, at large radial distance, where mostly pre-equilibrium particles are located, the radial momentum exhibits a different trend and is rapidly increasing with r.

In AMD calculations, the density profile in Fig. 7 shows a time evolution of the compression and expansion that is qualitatively similar to the BGBD case. However, we notice that AMD shows broader density distribution than BGBD as the system expands. The analysis of the radial momentum profile (Fig. 8) also reveals that the expansion dynamics in AMD is different from that in the BGBD case. When the system goes from the compressed state toward the normal density value ($t \approx 70$ fm/c), the collective momentum increases less than in the BGBD case. This suggests that the energy that was stored in compression goes into larger (with respect to BGBD) thermal kinetic fluctuations, which is consistent with the broader density profile observed in Fig. 7. It should be noticed that the broad density profile in the late stage does not mean homogeneous dilute matter but corresponds to the situation in which fragments are distributed widely in the space. By the comparison with the BGBD case, it seems that the system ceases to behave as homogeneous matter earlier, already at around $t = 70$ fm/c. Then, in contrast to what happens in the BGBD case, where the system is slowed down during the expansion phase, after $t = 70$ fm/c the expansion collective momentum remains almost unchanged in the AMD calculations. The mean-field restoring force, which would recompact the system, appears less effective in the event-averaged one-body dynamics. Moreover, after this time, the radial dependence of the collective momentum is almost self-similar for the "liquid" part. At all times, we see a kink in the $v(r)$ curve. The exterior and rapid component corresponds to the pre-equilibrium particles and the inner and slower component corresponds to the "liquid" composed mainly of fragments. However, the kink is always more pronounced in the BGBD case, pointing toward a larger difference of velocity between fragments and pre-equilibrium particles.

B. Fluctuations

The analysis of the density variance is an important tool for identifying the moment when fragmentation sets in and for obtaining some information about the related mechanism. The density variance has been widely used, in mean-field as well as in molecular dynamics calculations [7,41], to investigate the fragmentation path, in connection with the appearance of density bumps. During the fragmentation process, the density variance, evaluated at a given position $\mathbf{r}$, grows in time, then it saturates (when fragments no longer interact, apart from the Coulomb repulsion), and eventually it decreases as fragments fly apart from each other. For instance, in the spinodal decomposition scenario, the density fluctuations grow exponentially, with a characteristic amplification time τ (typically of the order of 30–50 fm/c) related to specific properties of the nuclear interaction such as its range [7].

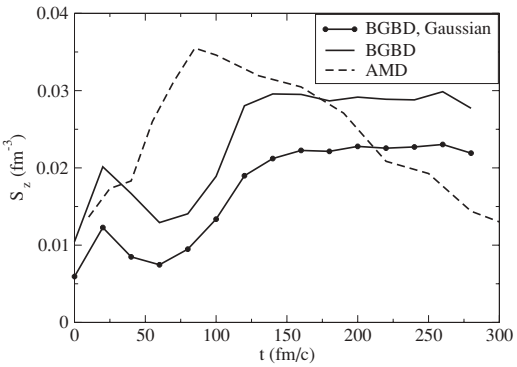

FIG. 9. Time evolution of the density variance averaged along the z direction, as obtained in BGBD (solid curve) and AMD (dashed curve) calculations. The curve with dots represents the results obtained in the BGBD case when artificially using the same Gaussian folding as in AMD.

Density variances have been calculated by starting from the value of the density along the x, y, and z axes. For instance, the variance of the density along the z axis is defined by $S_z^2(z) = \langle[\rho(0,0,z) - \langle\rho(0,0,z)\rangle]^2\rangle$, where $\rho(x,y,z)$ is the density for each event and the brackets $\langle\,\rangle$ stand for the average value over the event ensemble.

In Fig. 9 we show the time evolution of S_z, which is a representative value of $S_z(z)$, defined by

$$S_z = \frac{\int S_z(z)\langle\rho(0,0,z)\rangle dz}{\int\langle\rho(0,0,z)\rangle dz}. \tag{6}$$

This definition allows one to average the density variance inside the region where fragments are located. Similar behavior is observed for the variance in the transverse direction, whuch can be defined analogously, by averaging over x and y directions (see Fig. 10):

$$S_t = \frac{\int S_x(x)\langle\rho(x,0,0)\rangle dx + \int S_y(y)\langle\rho(0,y,0)\rangle dy}{\int\langle\rho(x,0,0)\rangle dx + \int\langle\rho(0,y,0)\rangle dy}. \tag{7}$$

One can see that density fluctuations have close values in the two approaches (compare sokid and dashed curves) in the high-density phase ($t \approx 40$ fm/c). However, in the BGBD case fluctuations are damped while the system expands, relaxing toward the lower equilibrium value expected for nuclear matter at lower density and temperature. Only when low-density values are reached ($t \approx 70$ fm/c) and the mean field is unstable does one start to see the rapid increase of density fluctuations, corresponding to fragment formation. This is because the density bumps are amplified, leading to fragments at normal density. When fragments fly apart from each other at large time t, the value of S gradually decreases from a trivial effect of its definition [Eqs. (6) and (7)].

However, in the AMD case the density fluctuations grow already as the system expands from $t \approx 40$ to 70 fm/c, suggesting that pre-fragments start to develop gradually at this stage even though the density is not very low. This is probably due to the nucleon wave packet localization when two-body scattering occurs. Indeed, early fragment formation has been observed also in other N-body treatments, belonging to the class of molecular dynamics models, as shown by the quasi-classical calculations performed in Ref. [13].

We would like to stress that the observation of the earlier growth of the density variance in the AMD case, with respect to the BGBD results, is not due to the different density smearing employed in the two models. In fact, when we evaluate the density in BGBD by artificially increasing the smearing width to the wave packet width of AMD, the density variance is reduced, as expected, but essentially exhibits the same trend (see the curve with dots in Figs. 9 and 10).

Also notice that S_z and S_t generally exhibit a similar behavior, though in the BGBD case the maximum fluctuation value reached along the z axis is smaller with respect to the transverse axis. This effect is not observed in AMD and is due to the lessee degree of stopping reached in BGBD.

As we have already mentioned, the relatively small magnitude of the collective momentum observed in Fig. 8 around $t \approx 70$ fm/c may be associated with the large momentum fluctuation. If the velocities of pre-fragments are randomly distributed, the collective momentum will fluctuate from one event to another. This is confirmed by the analysis of collective momentum fluctuations.

In fact, when the system is expanding ($t = 60$–70 fm/c), larger fluctuations are seen in the AMD case over the entire region where fragments are located, as shown in Fig. 11, where the collective momentum variance is displayed as a

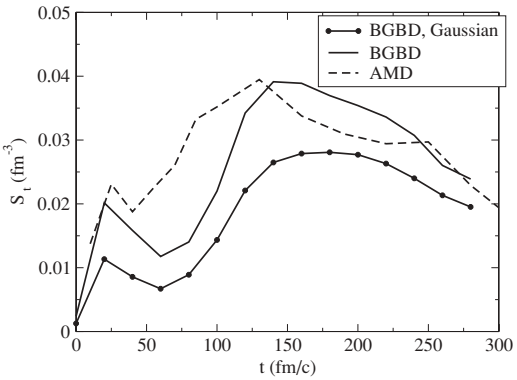

FIG. 10. Time evolution of the density variance averaged over the transverse direction. Notations are as in Fig. 9.

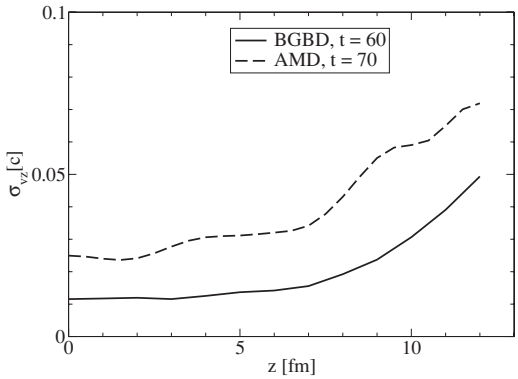

FIG. 11. Collective momentum variance, as obtained in BGBD (solid curve) and AMD (dashed curve) calculations, as a function of the distance on the z axis.

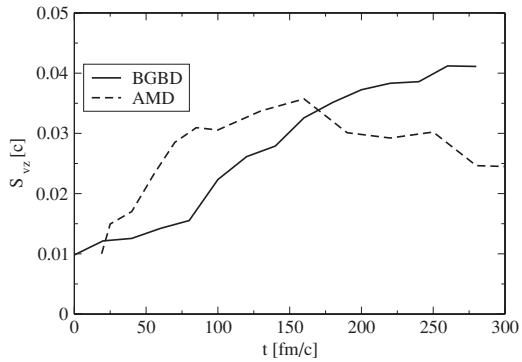

FIG. 12. Time evolution of the collective momentum variance, averaged along the z axis, as obtained in BGBD (solid curve) and AMD (dashed curve) calculations.

function of z. Furthermore, the mean-field restoring force for the global expansion dynamics is expected to be less effective in this situation and hence a deceleration of expansion is also weak in the AMD case, as observed by a comparison of Figs. 6 and 8.

To follow the development of the collective momentum fluctuations, in Fig. 12 we represent the time evolution of the collective momentum variance, averaged along the z axis, as in Eq. (6). Similarly to what has been seen for the density variance, in the AMD case momentum fluctuations are rapidly increasing, whereas in BGBD the steady increase of S_{vz} is essentially shifted in time, starting from $t \approx 70$ fm/c.

IV. DISCUSSION

According to the results presented here, emission mechanisms appear rather different in the two models. For light particles, a more abundant pre-equilibrium emission ($Z < 3$) is observed in the BGBD case. Concerning the IMF emission mechanism, the involved time scales and the relative importance of one- and many-body effects appear different in the two models, owing to the differences in the implementation of mean-field propagation and two-body scattering. In the BGBD case the fragmentation process follows the spinodal decomposition scenario. Indeed, the system enters the low-density region as a nearly homogeneous source, then density fluctuations are amplified. The formation of bubble-like structures is favored, as a manifestation of monopole instabilities [40]. In the AMD model, many-body correlations have a stronger impact on the fragmentation dynamics, while mean-field effects appear weaker. In fact, the density and momentum fluctuations grow earlier in AMD, suggesting that fragments are formed on shorter time scales in AMD, on about an equal footing as pre-equilibrium emission.

As shown in Fig. 9, spatial density fluctuations have similar values, in the high-density phase, in the two models. However, when the system starts to expand, fluctuations are quenched in BGBD (until mean-field instabilities are encountered) whereas they increase in AMD. The same is true for the collective momentum fluctuations (see Fig. 11). These differences are naturally understood as an effect of the nucleon localization in the AMD case, which induces larger many-body correlations. One can conclude that, in the energy range considered here (50 MeV/nucleon), the fragmentation path is extremely sensitive to the interplay between one- and many-body effects. Changing the relative weight of these effects leads to a rather different outcome.

As a consequence of the emission mechanisms outlined here, one expects to see different primary fragment configurations in the two models, with larger fluctuations in the AMD case, though results could be similar for inclusive observables, such as charge distributions, especially after secondary decay effects have been considered. For kinematic properties and more exclusive observables, such as IMF-IMF correlations, which keep better track of the freeze-out configuration and primary fragment partitions, one should be able to disentangle the predictions of the two models. In this respect, it would be particularly instructive to study fragment-size correlations, which, as shown in Refs. [5,42], may reveal the occurrence of spinodal instabilities in the fragmentation path. A comparison with available experimental data would allow some light to be shed on the mechanisms and most relevant effects that govern the fragmentation process. This analysis will be the subject of a forthcoming paper.

Also, it would be interesting to extend this study to semiperipheral collisions, to investigate transport properties and dissipation-equilibration mechanims. In charge-asymmetric reactions, isospin equilibration could be a good tracer of the reaction dynamics.

ACKNOWLEDGMENTS

We thank M. Di Toro for reading the manuscript and stimulating discussions. The AMD calculation was partly supported by the High Energy Accelerator Research Organization (KEK) as a supercomputer project.

[1] R. Botet, M. Ploszajczak, A. Chbihi, B. Borderie, D. Durand, and J. Frankland, Phys. Rev. Lett. **86**, 3514 (2001); J. D. Frankland *et al.*, contribution to the XLth Int. Winter Meeting on Nuclear Physics, Bormio (Italy), January 21–25, 2002.
[2] J. B. Elliott *et al.*, Phys. Rev. Lett. **88**, 042701 (2002).
[3] M. D'Agostino *et al.*, Nucl. Phys. **A699**, 795 (2002).
[4] Ph. Chomaz and F. Gulminelli, Nucl. Phys. **A647**, 153 (1999); F. Gulminelli, Ph. Chomaz, A. H. Raduta, and A. R. Raduta, Phys. Rev. Lett. **91**, 202701 (2003).
[5] G. Tabacaru *et al.*, Eur. Phys. J. A **18**, 103 (2003).
[6] A. Ono, Phys. Rev. C **59**, 853 (1999).
[7] Ph. Chomaz, M. Colonna, and J. Randrup, Phys. Rep. **389**, 263 (2004).
[8] H. S. Xu *et al.*, Phys. Rev. Lett. **85**, 716 (2000).
[9] E. Geraci *et al.*, Nucl. Phys. **A732**, 173 (2004).
[10] L. G. Sobotka, R. J. Charity, J. Toke, and W. U. Schroder. Phys. Rev. Lett. **93**, 132702 (2004).
[11] P. Bonche, S. Levit, and D. Vautherin, Nucl. Phys. **A436**, 265 (1985).
[12] P. Sapienza *et al.*, Phys. Rev. Lett. **87**, 072701 (2001).

[13] C. O. Dorso and J. Randrup, Phys. Lett. **B301**, 328 (1993).
[14] X. Campi, H. Krivine, and N. Sator, Nucl. Phys. **A681**, 458c (2001).
[15] F. Gulminelli and Ph. Chomaz, Phys. Rev. Lett. **82**, 1402 (1999).
[16] X. Campi, H. Krivine, E. Plagnol, and N. Sator, Phys. Rev. C **67**, 044610 (2003).
[17] J. Rizzo, M. Colonna, M. Di Toro, and V. Greco, Nucl. Phys. **A732**, 202 (2004).
[18] A. Ono, S. Hudan, A. Chbihi, and J. D. Frankland, Phys. Rev. C **66**, 014603 (2002).
[19] J. D. Frankland *et al*., Nucl. Phys. **A689**, 940 (2001).
[20] J. Aichelin, Phys. Rep. **202**, 233 (1991).
[21] H. Feldmeier, Nucl. Phys. **A515**, 147 (1990).
[22] A. Ono, H. Horiuchi, T. Maruyama, and A. Ohnishi, Phys. Rev. Lett. **68**, 2898 (1992); Prog. Theor. Phys. **87**, 1185 (1992).
[23] M. Papa, T. Maruyama, and A. Bonasera, Phys. Rev. C **64**, 024612 (2001).
[24] M. Colonna and Ph. Chomaz, Phys. Lett. **B436**, 1 (1998).
[25] S. Ayik and C. Gregoire, Phys. Lett. **B212**, 269 (1998), and references therein.
[26] J. Randrup and B. Remaud, Nucl. Phys. **A514**, 339 (1990).
[27] G. F. Bertsch and S. Das Gupta, Phys. Rep. **160**, 189 (1988).
[28] A. Bonasera, F. Gulminelli, and J. Molitoris, Phys. Rep. **243**, 1 (1994).
[29] A. Guarnera, M. Colonna, and Ph. Chomaz, Phys. Lett. **B373**, 267 (1996).
[30] V. Baran, M. Colonna, V. Greco, and M. Di Toro, Phys. Rep. **410**, 335 (2005).
[31] C. Gale, G. M. Welke, M. Prakash, S. J. Lee, and S. Das Gupta, Phys. Rev. C **41**, 1545 (1990).
[32] V. Greco, diploma thesis, University of Catania, Italy, 1997; V. Greco, A. Guarnera, M. Colonna, and M. Di Toro, Phys. Rev. C **59**, 810 (1999); Nuovo Cimento A **111**, 865 (1998).
[33] *Isospin Physics in Heavy-ion Collisions at Intermediate Energies*, edited by B.-A. Li and W. Udo Schröder (Nova Science, New York, 2001).
[34] I. Bombaci, in *Isospin Physics in Heavy-ion Collisions at Intermediate Energies*, edited by B.-A. Li and W. Udo Schröder (Nova Science, New York, 2001), p. 35 and references therein.
[35] M. Colonna *et al*., Nucl. Phys. **A642**, 449 (1998).
[36] M. Colonna *et al*., Nucl. Phys. **A742**, 337 (2004).
[37] A. Ono and H. Horiuchi, Prog. Part. Nucl. Phys. **53**, 501 (2004).
[38] J. Dechargé and D. Gogny, Phys. Rev. C **21**, 1568 (1980).
[39] A. Ono and H. Horiuchi, Phys. Rev. C **53**, 2958 (1996).
[40] G. Batko and J. Randrup, Nucl. Phys. **A563**, 97 (1993).
[41] S. Pratt, C. Montoya, and F. Ronning, Phys. Lett. **B349**, 261 (1995).
[42] B. Borderie *et al*., Phys. Rev. Lett. **86**, 3252 (2001).